*Journal of Applied Fluid Mechanics*, Vol. 11, No. 1, pp. 241-256, 2018.
Available online at www.jafmonline.net, ISSN 1735-3572, EISSN 1735-3645.
DOI: 10.29252/jafm.11.01.28235

# On the Instability of Two Dimensional Backward-Facing Step Flow using Energy Gradient Method

H. Nowruzi [1], S. Salman Nourazar [2†] and H. Ghassemi[1]

[1] *Department of Maritime Engineering, Amirkabir University of Technology, Tehran, Tehran, Iran*
[2] *Mechanical Engineering Department, Amirkabir University of Technology, Tehran, Tehran, Iran*

†*Corresponding Author Email: icp@aut.ac.ir*

(Received July 19, 2017; accepted August 23, 2017)

## ABSTRACT

In the present paper, the energy gradient method is implemented to study the instability of 2-D laminar backward-facing step (BFS) flow under different Reynolds numbers and expansion ratios. For this purpose, six different Reynolds numbers ($50 \leq \mathrm{Re} \leq 1000$) and two various expansion ratios of 1.9423 and 3 are considered. We compared our results of the present study with existing experimental and numerical data and good agreement is achieved. To study of fluid flow instability, we evaluated the distributions of velocity, vorticity and energy gradient function K. The results of our study show that as the expansion ratio decreases the flow becomes more stable. We also found that the origin of instability in the entire flow field is located on the separated shear layer nearby the step edge. In addition, we approved that the inflection point on the profile of velocity corresponds to the maximum of vorticity resulted to the instability.

**Keywords**: Energy gradient; Instability; Backward-facing step flow.

## NOMENCLATURE

| | | | |
|---|---|---|---|
| BFS | backward-facing step | $u$ | velocity component in $x$-direction |
| $D$ | hydraulic diameter | $U_{avg}$ | averaged velocity |
| $E$ | total mechanical energy | $U_{\max}$ | maximum of inlet velocity |
| FDM | Finite Difference Method | $v$ | velocity component in $y$-direction |
| $h_i$ | inlet height | $x$ | coordinate of $x$-direction |
| $h_s$ | step height | $x_1$ | main recirculation region |
| $h$ | half of the inlet height | $x_2$ | detachment length on the upper wall |
| $H$ | channel height at downstream of the step | $x_3$ | reattachment length on the upper wall |
| $H_L$ | energy lost | $Y$ | coordinate of $y$-direction |
| $K$ | dimensionless parameter of energy gradient method | | |
| $K_c$ | critical value of $K$ | $\alpha$ | angle of streamline related to $x$-direction |
| $L_I$ | inflow length | $\Delta y_{\min}$ | finest grid |
| $L_o$ | outflow length | $\mu$ | dynamic viscosity |
| $n$ | coordinate in transverse direction | $\upsilon$ | kinematic viscosity |
| $P$ | static pressure of flow field | $\rho$ | density |
| Re | Reynolds number | $\psi$ | stream function |
| $S$ | coordinate in stream-wise direction | $\omega$ | vorticity |

## 1. INTRODUCTION

Backward-facing step (BFS) flow is a classical issue in fundamental fluid mechanics. This flow geometry is a significant prototype to investigate of flow separation, flow reattachment and recirculation

bubbles. The phenomenon of flow separation is common in engineering applications, such as the water flow past the hydrofoil, the airflow past the blades of compressor and turbine, suddenly expanding pipes, combustors etc. (Rajasekaran 2011). The BFS geometry is also an important problem for understanding the instability of a separated flow.

In the literature, it is possible to find many numerical and experimental studies on the flow over a BFS. For example, Armaly *et al.* (1983) presented an experimental study on laminar, transitional and turbulent flows over the two-dimensional BFS in the Reynolds numbers range of $70 < Re < 8000$. Their experimental results show that the separation length at different Reynolds numbers specifies different flow regimes. Kaiktsis *et al.* (1991) performed a numerical investigation on the three-dimensional turbulent flow over a BFS. They indicated that Armaly *et al.* (1983) underestimated the recirculation lengths for Reynolds number above 600. In another study, Kaiktsis *et al.* (1996) claimed that the local convective instabilities produce the instability in BFS flow. Fortin *et al.* (1997) investigated the stability of the 2D steady incompressible flow over a BFS up to Re=1600. Their results show that the flow over a BFS is stable close to Reynolds number of 1600. Barkley *et al.* (2002) reported that the flow remains linearly stable to two-dimensional perturbations up to a Reynolds number of 1050. In addition, their results show no evidence of any nearby two-dimensional bifurcation up to Re=748. Beaudoin *et al.* (2004) simulated a three dimensional basic flow for understanding the origin of instabilities of the flow over a BFS. Their results show that, the vicinity of the reattached flow and outside the recirculation bubble are locations that have the most potential to being unstable.

Recently, several numerical and experimental studies in the field of BFS flow over various step angles (Bayraktar 2014), control of the reattachment length of a transonic 2D BFS flow (Bolgar *et al.* 2015), simulation of a gently curved BFS (Asgari and Tadjfar 2017), simulation of turbulent flows over a BFS by using a modified partially averaged Navier-Stokes model (Huang *et al.* 2017), heat transfer and fluid flow characteristics of separation and reattachment flow over a BFS (Xie and Xi 2017) and high intensity turbulent flow over a BFS (de la Torre *et al.* 2017) are conducted by scholars. For comparison between the cited works and to identify the novelty of current study, we present a summary of the cited works in Table 1.

As may be seen in Table 1, to our best of knowledge, the previous researchers did not consider the effect of the expansion ratios at different Reynolds numbers on the onset of instability in a BFS flow. In addition, the local positions in a BFS flow where the instability is originated from there, is not specified. Therefore, our goal in the present study is to investigate the instability (i.e. onset of instability and local positions in the BFS flow where the instability is originated from there) of 2D flow between parallel plates over a BFS under different Reynolds numbers and expansion ratios by using the energy gradient method (Dou 2004; Dou 2006). For this purpose, different Reynolds numbers ranging from 50 to 1000 and expansion ratios of 1.9423 and 3, are considered. The results of our investigation show that the onset of instability in a two-dimensional BFS flow is originated on the separated shear layer in the nearby the step edge.

## 2. PHYSICAL MODEL AND THE NUMERICAL METHOD

Figure 1 (a) shows the schematic of fully developed plane Poiseuille flow between parallel plates behind the BFS. The wake behind the BFS may be distinguished into six main regions namely, (I) separated shear layer, (II) corner eddy, (III) backflow zone or recirculation zone, (IV) reattachment zone, (V) redeveloping near-wall flow and (VI) relaxing outer layer shear (Rajasekaran 2011). Fig. 1 (b) also shows the schematic of intended computational domain for the BFS flow.

### 2.1 Governing Equations

In the present study, we consider a two-dimensional steady and laminar flow over a BFS. The incompressible and steady vorticity transport equation in Cartesian coordinates is:

$$u\frac{\partial \omega}{\partial x}+v\frac{\partial \omega}{\partial y}=\frac{\mu}{\rho}\left(\frac{\partial^2 \omega}{\partial x^2}+\frac{\partial^2 \omega}{\partial y^2}\right). \tag{1}$$

Where, $\rho$, $\mu$, $u$, $v$ and $\omega$ are density, dynamic viscosity, velocity component in $x$-direction, velocity component in $y$-direction and the vorticity, respectively. We define the stream function $\psi$ and the vorticity function $\omega$ as:

$$\frac{\partial \psi}{\partial x}=-v \tag{2}$$

$$\frac{\partial \psi}{\partial y}=u \tag{3}$$

The definition of vorticity is:

$$\frac{\partial v}{\partial x}-\frac{\partial u}{\partial y}=\omega. \tag{4}$$

So, combining Eqs. (2-4), we obtain:

$$\frac{\partial^2 \psi}{\partial x^2}+\frac{\partial^2 \psi}{\partial y^2}=-\omega. \tag{5}$$

By substituting Eq. (2) and Eq. (3) into the vorticity transport equation (Eq. (1)), we obtain the following expression:

**Table 1 Summary of the cited works in the field of BFS flows.**

| Author | Technique | Conditions | Evaluated criteria |
|---|---|---|---|
| Armaly *et al.* (1983) | experimental & numerical | 70 < Re < 8000<br>ER*= 1.9423 | velocity profile<br>detachment & reattachment lengths |
| Kim and Moin (1985) | numerical | 100 < Re < 800<br>ER= 1.9423 | detachment and reattachment lengths |
| Gartling (1990) | numerical | Re =800<br>ER= 1.9423 | stream function and vorticity<br>velocity profile<br>pressure distribution |
| Kaiktsis *et al.* (1991) | numerical | 50 < Re < 800<br>ER= 1.9423 | stream function and vorticity<br>velocity profile |
| Kaiktsis *et al.* (1996) | numerical | 700 < Re < 2500<br>ER= 2 | velocity profile<br>stability analysis by using linear stability method |
| Fortin *et al.* (1997) | numerical | 100 < Re < 1500<br>ER= 2 | stability analysis through the study on the localization of Hopf bifurcations |
| Chiang and Sheu (1999) | numerical | 100 < Re < 1000<br>ER= 1.9423 | velocity profile<br>detachment & reattachment lengths |
| Barkley *et al.* (2002) | numerical | 450 < Re < 1050<br>ER= 2 | detachment & reattachment lengths<br>stability analysis by using linear stability calculations |
| Beaudoin *et al.* (2004) | experimental & numerical | 50 < Re < 500<br>ER=1.11 | detachment & reattachment lengths<br>stability analysis through the study the onset of 2D instability by using generalized Rayleigh discriminant |
| Biswas *et al.* (2004) | numerical | 0 < Re < 500<br>ER=1.9423, 2.5 and 3 | pressure loss<br>detachment & reattachment lengths<br>velocity profile and streamlines |
| Blackburn *et al.* (2008) | numerical | 0 < Re < 500<br>ER= 2 | stability analysis through the study the onset of asymptotic instability by using linear perturbations |
| Erturk (2008) | numerical | 100 < Re < 3000<br>ER=1.9423 | velocity profile<br>detachment & reattachment lengths |
| Bolgar *et al.* (2015) | experimental | Re=180000 | stream-wise vortex<br>detachment & reattachment lengths |
| Li *et al.* (2017) | numerical | $5\times10^3$ <Re< $64\times10^3$<br>ER=1.28, 2, 3.27 | velocity profile<br>detachment & reattachment lengths |
| Asgari and Tadjfar (2017) | numerical | Re=13700 | velocity profile<br>pressure coefficient and fluctuation<br>detachment & reattachment lengths |
| Huang *et al.* (2017) | numerical | Re = 5000 | pressure loss and skin friction<br>detachment & reattachment lengths<br>velocity profile and streamlines |
| Xie and Xi (2017) | numerical | 400 < Re < 1000<br>ER=1.5, 2 and 2.5 | temperature fields and Nusselt number<br>detachment & reattachment lengths<br>velocity profile and streamlines |
| de la Torre *et al.* (2017) | experimental | $15\times10^3$<Re<$64\times10^3$ | velocity profile |

* ER=expansion ratio

$$\frac{\partial \psi}{\partial y}\frac{\partial \omega}{\partial x}-\frac{\partial \psi}{\partial x}\frac{\partial \omega}{\partial y}=\frac{\mu}{\rho}\left(\frac{\partial^2 \omega}{\partial x^2}+\frac{\partial^2 \omega}{\partial y^2}\right). \quad (6)$$

We discretized equations (Eqs. (2 - 6)) by using the finite difference method (FDM). In addition, the Reynolds number may be defined as $Re=\left(D.U_{avg}\right)/\upsilon$, where $U_{avg}$, $D$ and $\upsilon$ are the average velocity at the inlet, hydraulic diameter and kinematic viscosity, respectively. In the present study, the hydraulic diameter of the inlet channel ($D$) is equivalent to twice the inflow channel height ($D=2h_i$).

## 2.2 Energy Gradient Method

Dou (2006) proposed the energy gradient method based on Newtonian mechanics to investigate of the flow instability. This theory has two laws. First law of energy gradient state that, if a material system is static, when the energy gradient in some direction is larger than a critical value, the system will become unstable and the phase change or flow would occur. Second law of energy gradient is also express that,

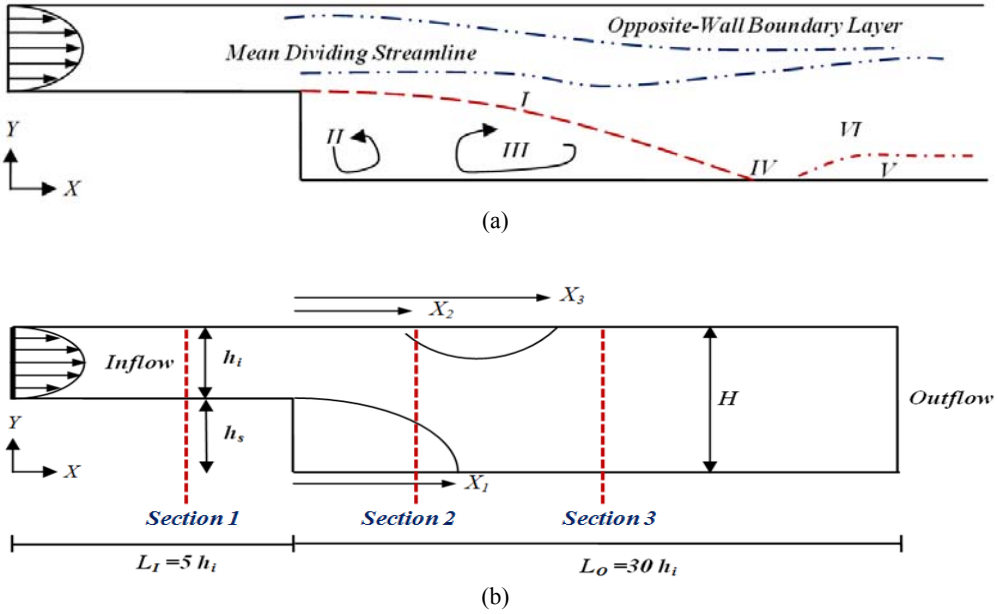


**Fig. 1. (a) Flow characteristics behind the BFS, (b) Schematic of the BFS flow, length scale and definition of three computational sections.**

if a material system flows, when the ratio of the energy gradient in the transverse direction and that in the stream-wise direction is larger than a critical value, the system will become unstable (Dou 2004; Dou 2006).

In energy gradient method, to investigate of fluid flow stability, Dou *et al.* (2006) proposed a dimensionless parameter $K$ as (Dou 2004)

$$K = \frac{\partial E / \partial n}{\partial H_L / \partial s}. \tag{7}$$

Where, $\partial E / \partial n$ and $\partial H_L / \partial s$ are representative of energy gradient in transverse (or cross-stream) direction and energy gradient in stream-wise direction, respectively. In addition, $E = P + 0.5\rho U^2$ is the total mechanical energy per unit volumetric fluid ($P$ is static pressure of flow field and $U$ is total velocity ($U = \sqrt{u^2 + v^2}$)). Moreover, $H_L$, $n$ and $s$ are energy lost, cross-stream direction of the streamline and stream-wise direction along the streamline, respectively. Based on energy gradient method (Dou 2004; Dou 2006), energy gradient in transverse direction amplitude the instability, whereas, energy gradient in stream-wise direction with role of viscosity friction decay the flow instability. Therefore, based on the energy gradient method (Dou 2004; Dou 2006), where $K$ is greater than the critical parameter $K_c$, fluid flow becomes unstable.

In the case of BFS flow, Eq. (7) may be written as (Dou 2008):

$$K = \frac{\partial E / \partial n}{\partial H / \partial s} = \frac{\dfrac{\partial\left(P + \frac{1}{2}\rho U^2\right)}{\partial n}}{\dfrac{\partial\left(P + \frac{1}{2}\rho U^2\right)}{\partial s}} = \frac{\rho\left(\vec{U} \times \vec{\omega}\right).\dfrac{d\vec{n}}{|d\vec{n}|} + \left(\mu\nabla^2\vec{U}\right).\dfrac{d\vec{n}}{|d\vec{n}|}}{\rho\left(\vec{U} \times \vec{\omega}\right).\dfrac{d\vec{s}}{|d\vec{s}|} + \left(\mu\nabla^2\vec{U}\right).\dfrac{d\vec{s}}{|d\vec{s}|}}. \tag{8}$$

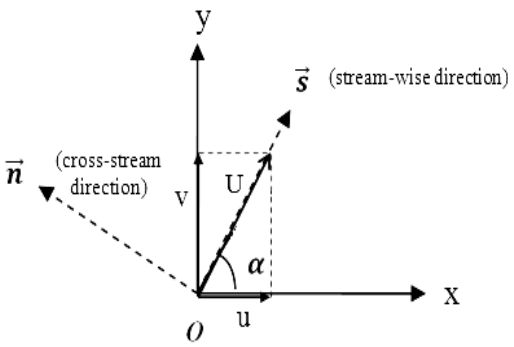


**Fig. 2. Geometrical schematic of stream-wise and cross-stream coordinates system.**

Substituting Eq. (9) into the Eq. (8), we obtain

Figure 2 shows geometrical schematic of stream-wise and normal coordinates system. According to Fig. 2, we obtain the following expressions (Dou and Ben 2015):

$$\begin{cases} \cos\alpha = \dfrac{u}{U}, \quad \sin\alpha = \dfrac{v}{U} \\ \dfrac{d\vec{n}}{|d\vec{n}|} = (-\sin\alpha, \cos\alpha) \\ \dfrac{d\vec{s}}{|d\vec{s}|} = (\cos\alpha, \sin\alpha) \\ \omega_z = \dfrac{\partial v}{\partial x} - \dfrac{\partial u}{\partial y}, \quad \vec{U} \times \vec{\omega} = (v\omega_z, u\omega_z) \end{cases} \tag{9}$$

the following expression for dimensionless parameter $K$ as (Dou and Ben 2015):

$$K = \frac{\partial E/\partial n}{\partial H/\partial s} = \frac{\mu\left(\frac{\partial^2 v}{\partial x^2} + \frac{\partial^2 v}{\partial y^2}\right)\cos\alpha - \mu\left(\frac{\partial^2 u}{\partial x^2} + \frac{\partial^2 u}{\partial y^2}\right)\sin\alpha}{\mu\left(\frac{\partial^2 v}{\partial x^2} + \frac{\partial^2 v}{\partial y^2}\right)\sin\alpha + \mu\left(\frac{\partial^2 u}{\partial x^2} + \frac{\partial^2 u}{\partial y^2}\right)\cos\alpha} - \frac{-\rho v\omega_z \sin\alpha - \rho u\omega_z \cos\alpha}{\mu\left(\frac{\partial^2 v}{\partial x^2} + \frac{\partial^2 v}{\partial y^2}\right)\sin\alpha + \mu\left(\frac{\partial^2 u}{\partial x^2} + \frac{\partial^2 u}{\partial y^2}\right)\cos\alpha} \tag{10}$$

In order to investigate of flow instability in a BFS flow, we implement the following three-steps under considered Reynolds numbers and expansion ratios:

Step1. Compute of velocity component, stream function and vorticity by using Eqs. (2-6).

Step2. Calculate of dimensionless parameter of energy gradient method ($K$) by using Eq.(10) throughout of our computational domain.

Step3. Plot the vorticity and $K$ contours together with velocity, vorticity and $K$ profiles and detect of critical local positions in the BFS domain with highest value of dimensionless parameter of energy gradient method ($K_{max}$).

## 2.3 Geometric Model and Boundary Conditions

Figure 1(b) shows the schematic of intended computational domain for the BFS flow and it is in accordance with the experimental setup of Armaly *et al.* (1983). As may be seen in Fig.1 (b), the coordinate system is located in the down corner and its axes are parallel to the channel sides.

The expansion ratio is defined by $H / h_i$, which is the ratio of channel height at downstream of the step ($H$) per height of the inflow channel ($h_i$). In the current study, we consider two expansion ratios of 1.9423 and 3. All of the geometrical length scales in the computational domain are dimensionless according to the channel height ($h_i$). We set the large enough channel length at the upstream and downstream for minimizing the impressions of the outflow boundary on the upstream zones (Biswas *et al.* 2004; Kosma 2005). Channel length at the upstream and downstream are equal to $L_I = 5h_i$ and $L_O = 30h_i$, respectively. Moreover, Fig. 1 (b) presents the length of the main recirculation region ($X_1$) and the detachment and reattachment locations of the first recirculation region on the upper wall (i.e. $X_2$ and $X_3$).

We consider a standard parabolic velocity profile $u(y) = 4U_{max}\dfrac{y(h_i - y)}{h_i^2}$ with maximum inflow velocity of $U_{max} = 1.5U_{avg}$ and an average inflow velocity of $U_{avg} = 1$ at upstream of the backward facing step flow. We use zero diffusion flux and no-slip fixed wall boundary conditions for the outlet and on the walls of our computational domain, respectively (Li *et al.* 2017).

## 2.4 Mesh Sensitivity Analysis and Validation Study

We conduct an extensive mesh sensitivity analysis to investigate that our computed results are grid independent. For this purpose, in the present section, grid independency tests for Re=100, Re=800 and Re=1000 at expansion ratio of $H / h_i = 1.9423$ are presented. For mesh sensitivity analysis, seven different structured meshes from finest grid ($\Delta y_{min} = 0.002$) to coarsest grid ($\Delta y_{min} = 0.15$) are tested. We select the length of the main recirculation region per step height ($X_1 / h_s$) to validate our results with Armaly *et al.* experiment data (Armaly *et al.* 1983). Fig. 3 shows that our results are in good agreement with the result of Armaly *et al.* experimental data (Armaly *et al.* 1983).

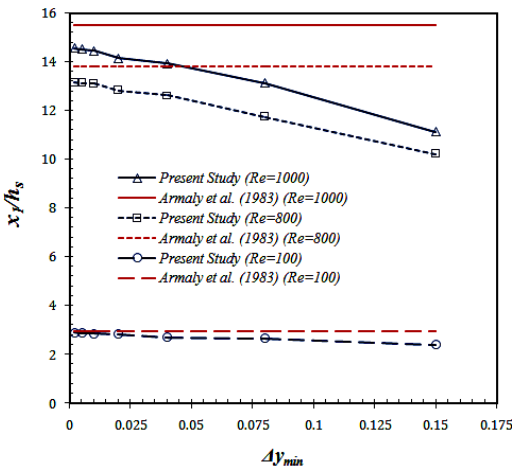


**Fig. 3. Grid independence tests based on the length of the main recirculation region $X_1 / h_s$ for expansion ratio of $H / h_i = 1.9423$ and Reynolds numbers 100, 800 and 1000.**

**Table 2 Detachment and reattachment lengths of the flow under different Reynolds numbers ranging from 50 to 1000 at $H / h_i = 1.9423$**

| Case | | Reynolds number | | | | | |
|---|---|---|---|---|---|---|---|
| | | 50 | 100 | 300 | 500 | 800 | 1000 |
| $X_1$ | present study | 1.750 | 2.765 | 6.125 | 8.422 | 13.120 | 14.521 |
| | Erturk (2008) | - | 2.878 | 6.659 | 9.437 | 11.983 | 13.267 |
| $X_2$ | present study | 0 | 0 | 0 | 7.538 | 8.115 | 9.281 |
| | Erturk (2008) | - | 0 | 0 | 8.314 | 9.646 | 10.592 |
| $X_3$ | present study | 0 | 0 | 0 | 11.020 | 18.250 | 21.680 |
| | Erturk (2008) | - | 0 | 0 | 12.504 | 19.992 | 24.275 |

**Table 3 Detachment and reattachment lengths of the flow under different Reynolds numbers ranging from 50 to 1000 at $H / h_i = 3$**

| Case | | Reynolds number | | | | | |
|---|---|---|---|---|---|---|---|
| | | 50 | 100 | 300 | 500 | 800 | 1000 |
| $X_1$ | present study | 3.865 | 6.365 | 9.685 | 10.810 | 13.825 | 14.355 |
| | Biswas *et al.* (2004) | 3.766 | 6.277 | 10.744 | - | - | - |
| $X_2$ | present study | 0 | 0 | 7.325 | 8.250 | 8.780 | 9.929 |
| $X_3$ | present study | 0 | 0 | 16.625 | 14.125 | 19.125 | 22.650 |

According to Fig. 3, $\Delta y_{min} = 0.01$ is selected due to convergence of our results after this grid density. Based on this selected grid, we achieved relative error between our numerical results with experiment data (Armaly *et al.* 1983) equal to 3.8% , 5.3% and 7.1% in respective for Re=100, Re=800 and Re=1000.

## 3. RESULTS AND DISCUSSION

Numerical results of detachment and reattachment lengths of the flow under different Reynolds numbers ranging from 50 to 1000 and expansion ratios at $H / h_i = 1.9423$ and 3 are reported in Tables 2 and 3, respectively. To measure the detachment and reattachment lengths, we shift the coordinate system to lower corner of the step. In addition, in Tables 2 and 3, we compare our results with existing numerical data (Biswas *et al.* 2004; Erturk 2008). Based on Table 2, the comparison of our results with the Erturk (2008) data shows that there is a reasonable agreement for the detachment and the reattachment lengths. Table 3 shows that the main recirculation region ($X_1$) is in good agreement with the result of Biswas *et al.* (2004) numerical data. By comparing Table 2 with Table 3, we also find that the greater expansion ratios lead to larger detachment and reattachment lengths.

Figure 4 displays the distribution of vorticity under different Reynolds numbers ranging from 50 to 1000 and expansion ratios of $H / h_i = 1.9423$ and $H / h_i = 3$. As shown in Fig. 4, the formation of separated shear layer and eddies in the backflow zone occur as soon as flow separation takes place at the step edge of the BFS flow. Moreover, Fig. 4 shows that the opposite wall boundary layer as defined in Fig. 1(a) is visible for Reynolds number above 300 at both expansion ratios of $H / h_i = 1.9423$ and $H / h_i = 3$. Fig. 4 also shows that the increase of expansion ratio leads to growth in the size of separated shear layer.

Figure 5 presents the contour of dimensionless parameter $K$ (the parameter that indicates the onset of instability) under different Reynolds number ranging from 50 to 1000 and both expansion ratios of 1.9423 and 3. As shown in Fig. 5, the distribution of $K$ contour at the upstream flow complies with the data of Dou *et al.* (2008) study using the energy gradient method (Dou 2008). Fig. 5 also shows that the maximum values of $K$ are located in the separated shear layer for Reynolds numbers ranging from 50 to 1000 and expansion ratios of $H / h_i = 1.9423$ and $H / h_i = 3$. Based on this result, we expect the onsets of initial instabilities at shear layer. This observation is consistent with the process of vortex roll up and the pairing mechanism in the separated shear layer which is reported by Troutt *et al.* (1984). In addition, Fig. 5 shows that the maximum values of $K$ increase with an increase in the expansion ratio.

| Re | $H / h_i$ = 1.9423 | $H / h_i$ = 3 |
|---|---|---|
| 50 | 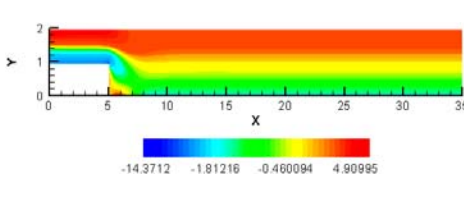 | 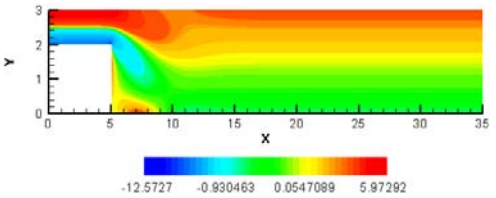 |
| 100 | 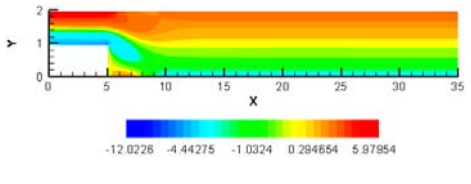 | 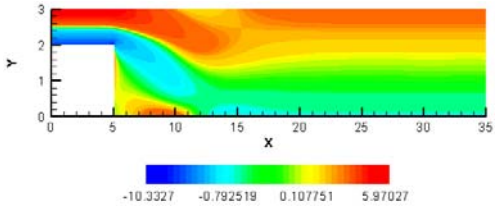 |
| 300 | 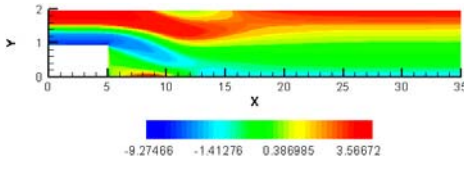 | 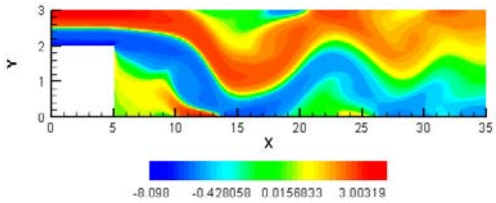 |
| 500 | 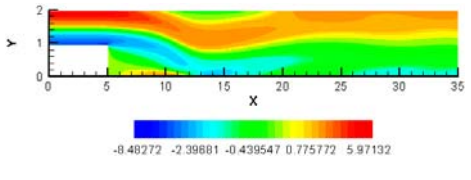 | 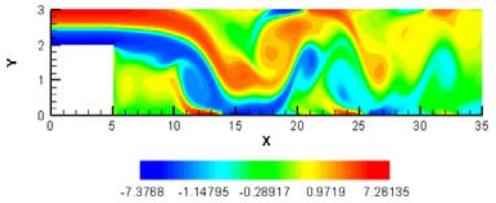 |
| 800 | 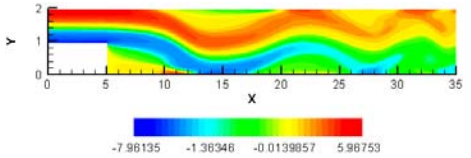 | 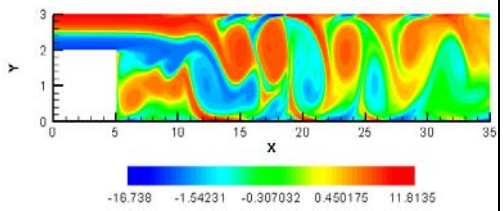 |
| $10^3$ | 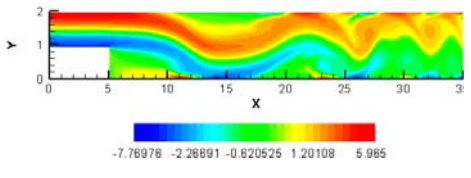 | 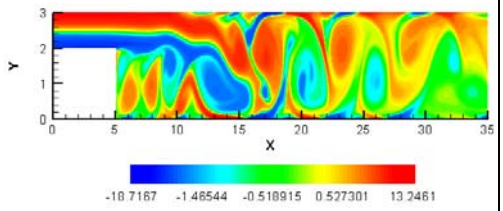 |

**Fig. 4. Distribution of vorticity under different Reynolds numbers ranging from 50 to 1000 and expansion ratios of $H / h_i = 1.9423$ and $H / h_i = 3$ .**

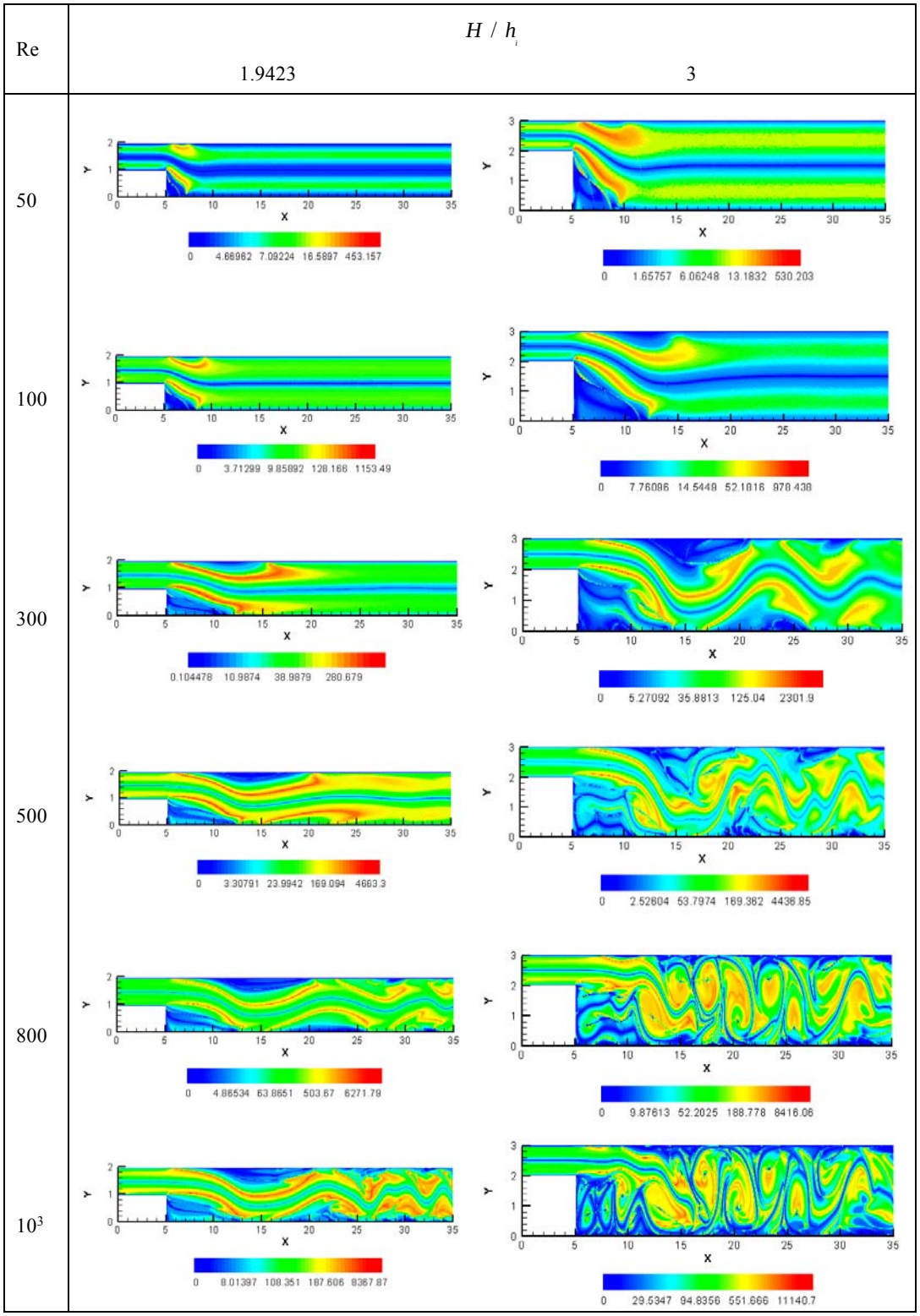


**Fig. 5. Distribution of $K$ under different Reynolds numbers ranging from 50 to 1000 and expansion ratios of $H / h_i = 1.9423$ and $H / h_i = 3$ .**

As may be seen in Fig.1 (b), we consider three different sections along our computational domain, sections 1, 2 and 3 which are located at X=2.5, X=7.5 and X=17.5, respectively.

Figurs 6 and 7 display the distribution of velocity, vorticity and dimensionless parameter $K$ at section 1 (X=2.5) under different Reynolds numbers ranging from 50 to 1000 and expansion ratios of $H / h_i = 1.9423$ and $H / h_i = 3$, respectively. As shown in Fig.6, the maximum values of $K$ at

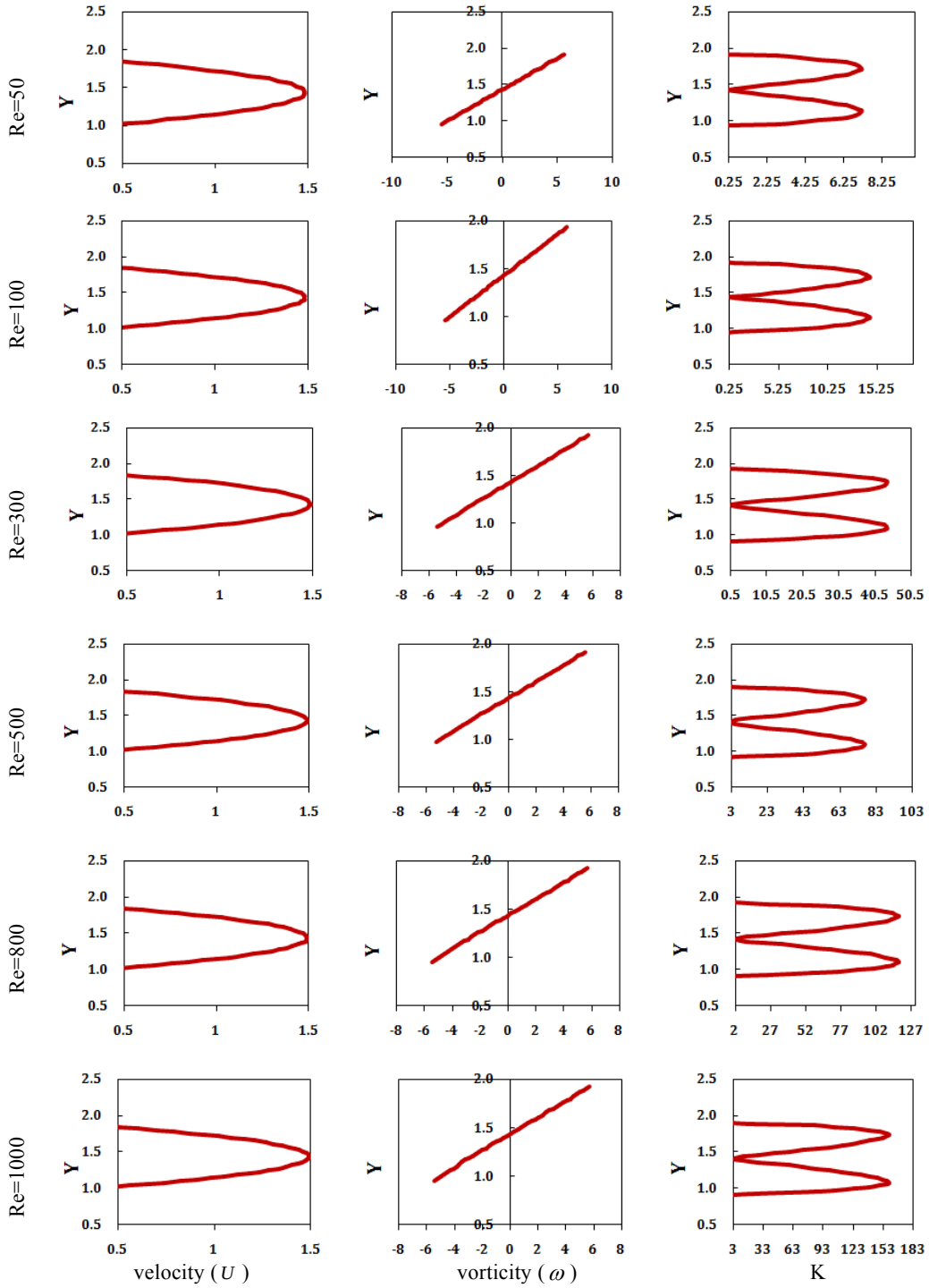


**Fig. 6. Distribution of velocity, vorticity and $K$ at section 1 under different Reynolds numbers ranging from 50 to 1000 and expansion ratio of $H / h_i = 1.9423$.**

expansion ratio of $H / h_i = 1.9423$ occur at $Y = 1.772$ and $Y = 1.192$. Fig. 7 shows that the maximum values of $K$ at expansion ratio of $H / h_i = 3$ are located at $Y = 2.830$ and $Y = 2.253$. Also, our results related to the locations of the maximum values of $K$ which are extracted from Figs. 6 and 7 are in good agreement with the results of Nishioka *et al.* experimental data (Nishioka *et al.* 1975) and Farahbakhsh *et al.* (2014) numerical data (it should be noted that origin of Y-coordinate in our study is $h_s + 0.5h_i$ compared to Nishioka *et al.* (1975) experiment and Farahbakhsh *et al.* (2014) numerical data).

Moreover, as may be seen in Fig.6 and Fig.7, growth of Reynolds number resulted to increase of

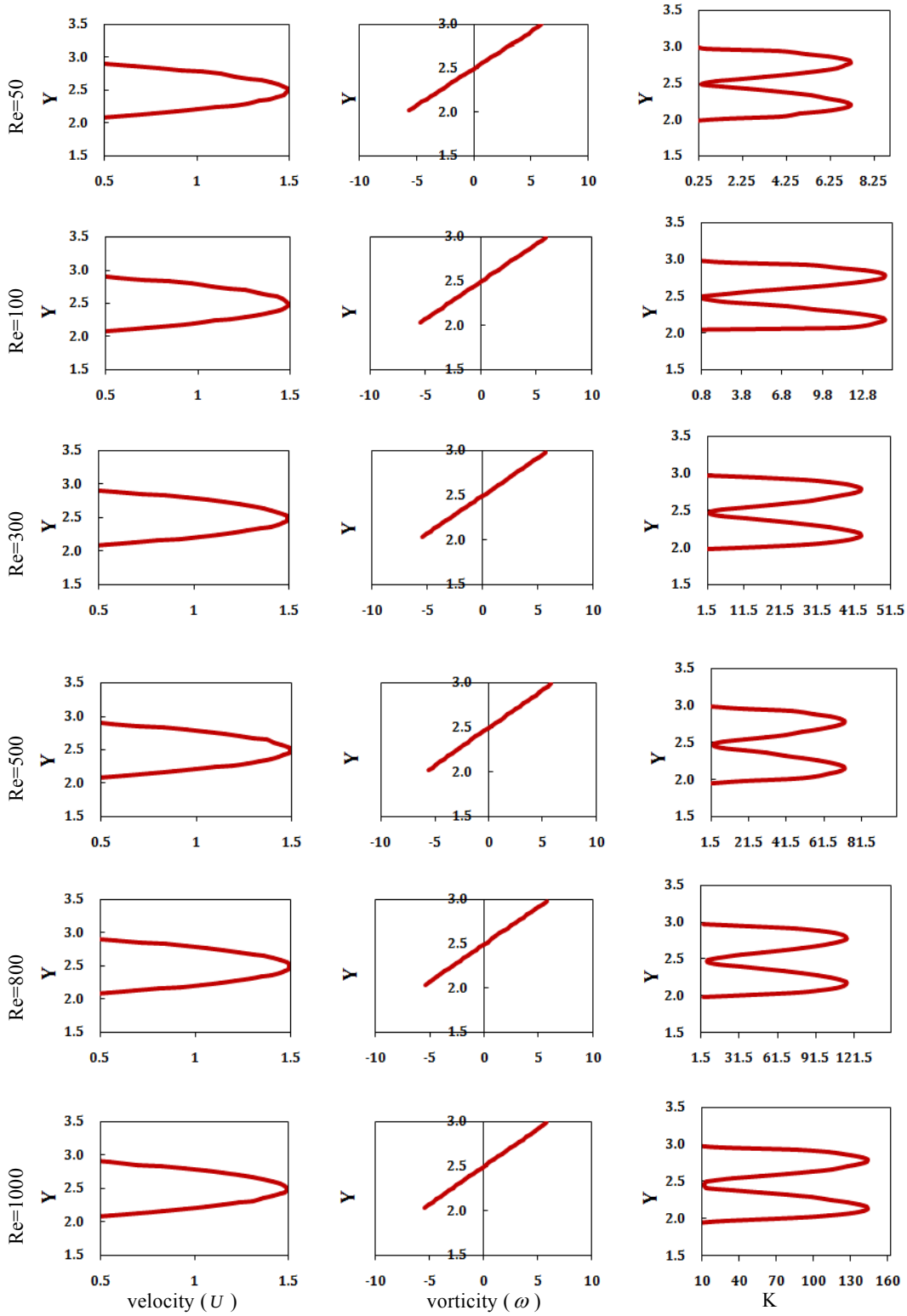


**Fig. 7. Distribution of velocity, vorticity and $K$ at section 1 under different Reynolds numbers ranging from 50 to 1000 and expansion ratio of $H / h_i = 3$.**

the maximum of $K$ value. By comparison between Fig.6 and Fig.7, similar trends in velocity, vorticity and $K$ is observable. The reason of this fact is related to same value of inflow height and similar upstream plane Poiseuille flow for both expansion ratios of $H / h_i = 1.9423$ and $H / h_i = 3$. Also, it is found that the minimum of $K$ value is located where the maximum of velocity profile is in correspondence to zero value of vorticity.

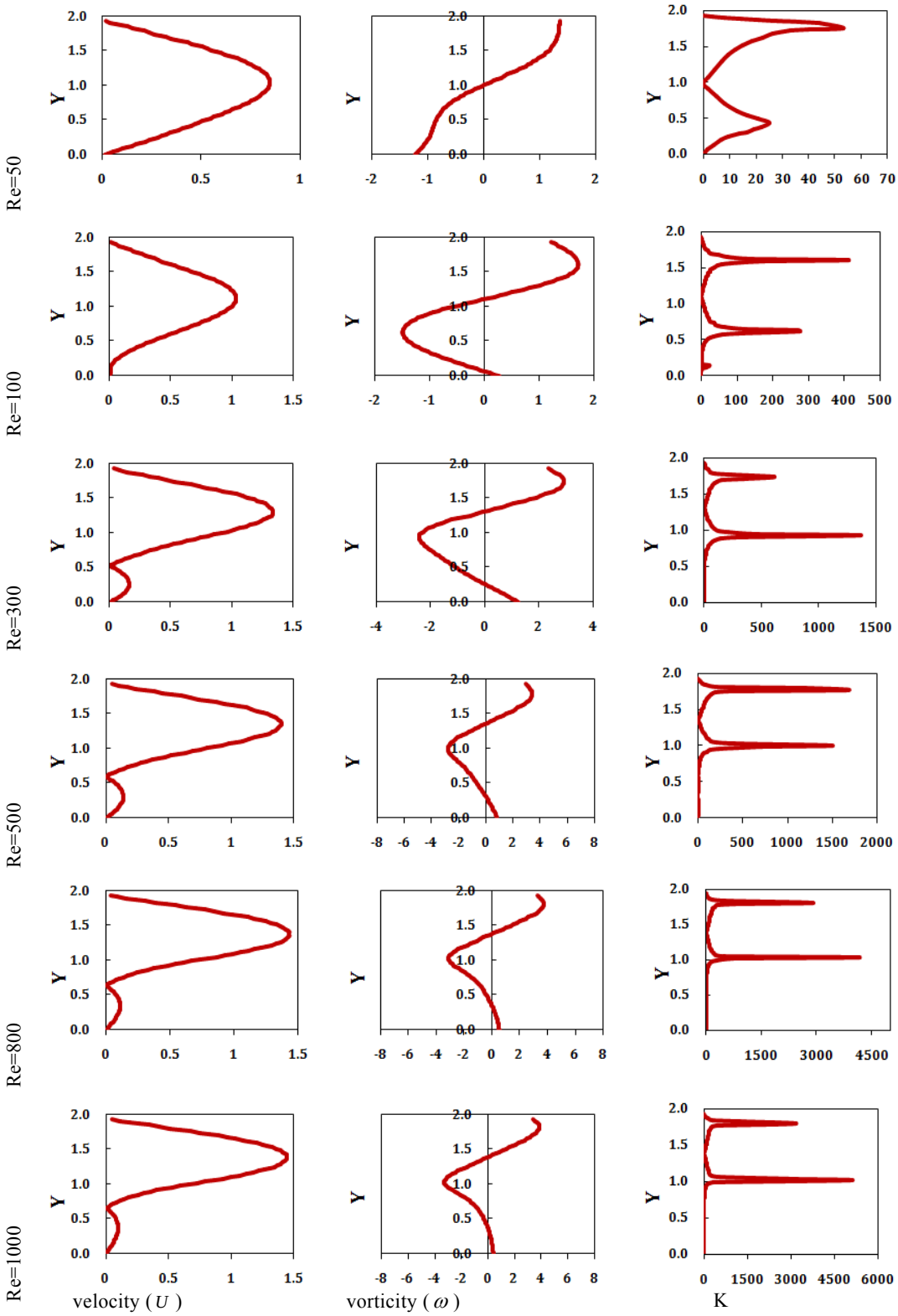


**Fig. 8. Distribution of velocity, vorticity and *K* at section 2 at different Reynolds numbers ranging from 50 to 1000 and expansion ratio of $H / h_i = 1.9423$ .**

Moreover, maximum of *K* value occurs at the position with inflection point in velocity profile and maxima of vorticity.

Based on *K* contour in Fig.5, we found that *K* at the corner eddy and recirculation zone is remarkably low. This means that the corner eddies and recirculation zone have no impression on the flow instability. To better understanding of this phenomenon, Figs. 8 and 9 present the distribution

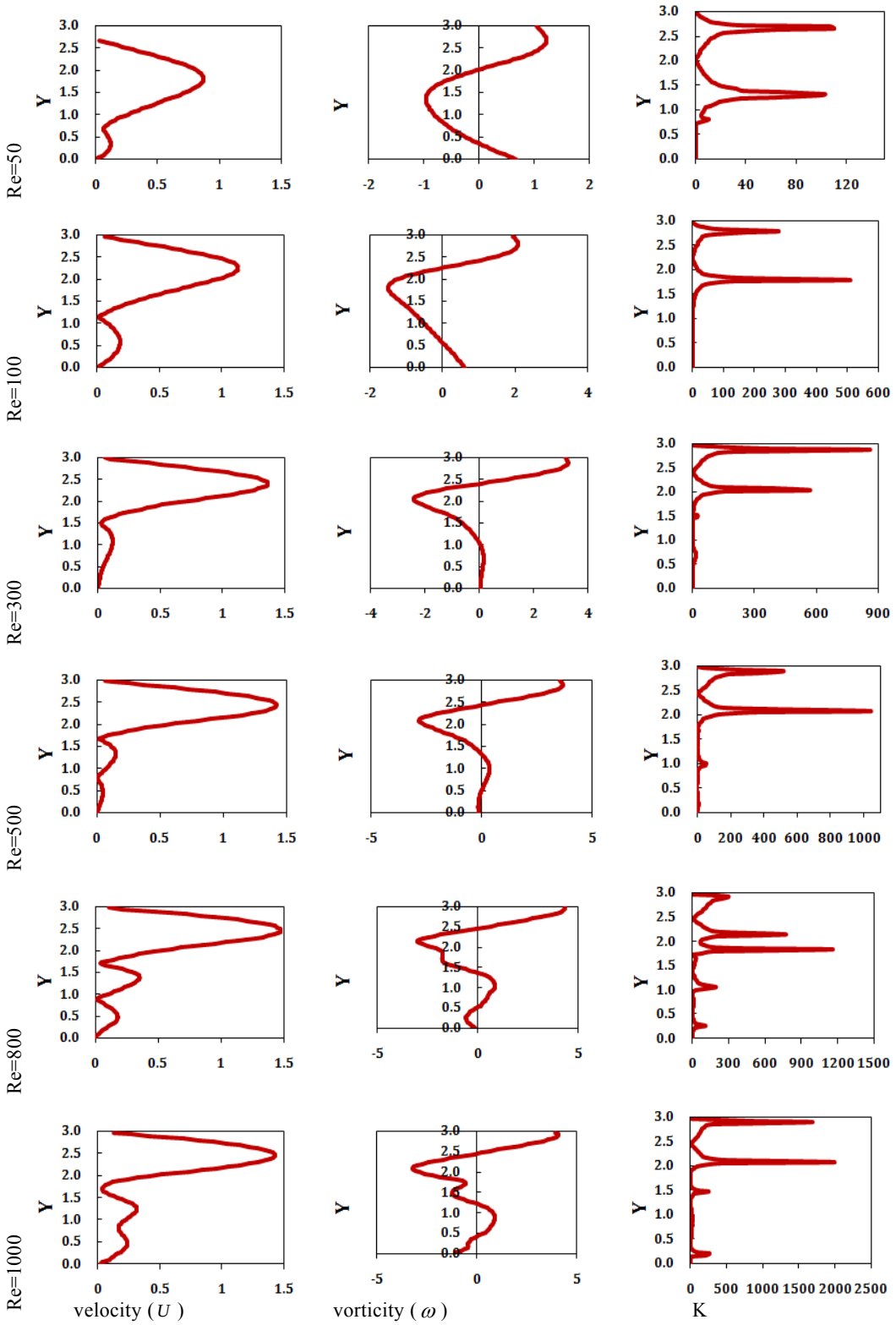


**Fig. 9. Distribution of velocity, vorticity and $K$ at section 2 at different Reynolds numbers of ranging from 50 to 1000 and expansion ratio of $H / h_i = 3$ .**

of velocity, vorticity and dimensionless parameter $K$ at section 2 (X=7.5) at different Reynolds numbers ranging from 50 to 1000 and expansion ratios of $H / h_i = 1.9423$ and $H / h_i = 3$, respectively. As may be seen from Figs. 8 and 9, we found that the maximum values of $K$ are located in the position of inflection point for Reynolds numbers ranging from 50 to 1000 and both

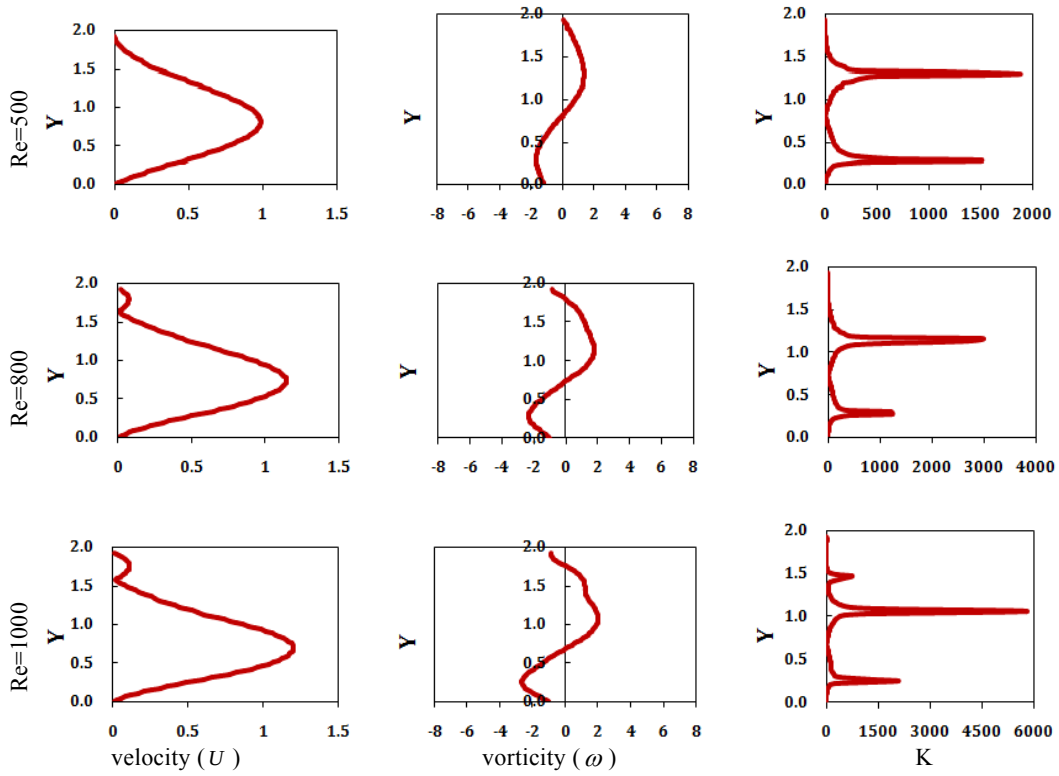


**Fig. 10. Distribution of velocity, vorticity and $K$ at section 3 at different Reynolds numbers ranging from 500 to 1000 and expansion ratio of $H / h_i = 1.9423$.**

expansion ratios of $H / h_i = 1.9423$ and $H / h_i = 3$.

By comparing between Figs. 8 and 9 with Fig.5, one can be concluded that, parameter $K$ has highest value at the shear layer. However, parameter $K$ has low value at corner eddies and recirculation zones is low. So, chance of onset of instability in corner eddies and a recirculation zone is negligible. Also, it is found that, for all Reynolds number, the maximum of $K$ is located at the position of inflection point. Indeed, we have maximum of $K$, where the second derivative of velocity is zero corresponding with maxima of vorticity.

To detail investigation on the fluid flow behavior at the redeveloping near-wall flow and relaxing outer layer shear, we present Figs. 10 and 11 to show the distribution of velocity, vorticity and dimensionless parameter $K$ at section 3 (X=17.5) at different Reynolds numbers ranging from 500 to 1000 and expansion ratios of $H / h_i = 1.9423$ and $H / h_i = 3$, respectively. By comparison between the K contour in Fig.5 with Figs.10 and 11, one can be concluded that, maximum of $K$ value is located in the position where two separating shear layers at upper and lower of downstream are interacted together. In addition, as may be seen from Figs.10 and 11, the maximum values of $K$ corresponds the position of inflection point. This phenomenon is also reported by Dou and Ben (2015). The reason of this phenomenon is related to maximum of 2D vorticity that occur at $\frac{\partial \omega_z}{\partial y} = \frac{\partial^2 v}{\partial x \partial y} - \frac{\partial^2 u}{\partial y^2} = 0$, where due to low value of $\frac{\partial^2 v}{\partial x \partial y}$ in case of BFS, we can approximate $\frac{\partial \omega_z}{\partial y}$ by $\frac{\partial^2 u}{\partial y^2} = 0$. Here, $\frac{\partial^2 u}{\partial y^2} = 0$ is representative of inflection point in the velocity profile.

Table 4 presents the value of $K_{max}$ and its position, in XY-coordinates as defined in Fig.1 (b), in the entire flow field at different Reynolds numbers ranging from 50 to 1000 and expansion ratios of $H / h_i = 1.9423$ and $H / h_i = 3$.

As may be seen from Table 4, for Re ≥ 100, as the expansion ratio increases, the values of $K_{max}$ become greater. Therefore, one can concluded that, in the positions with $K_{max}$, the energy gradient in cross-stream direction is significantly larger than energy gradient in stream-wise direction (i.e. viscosity friction). Table 4 also shows that the position of $K_{max}$ is located nearby the edge for Reynolds numbers ranging from 50 to 1000 and expansion ratios of $H / h_i = 1.9423$ and $H / h_i = 3$.

The physical reason of this happen is related to enhancement of pressure drop with increase of

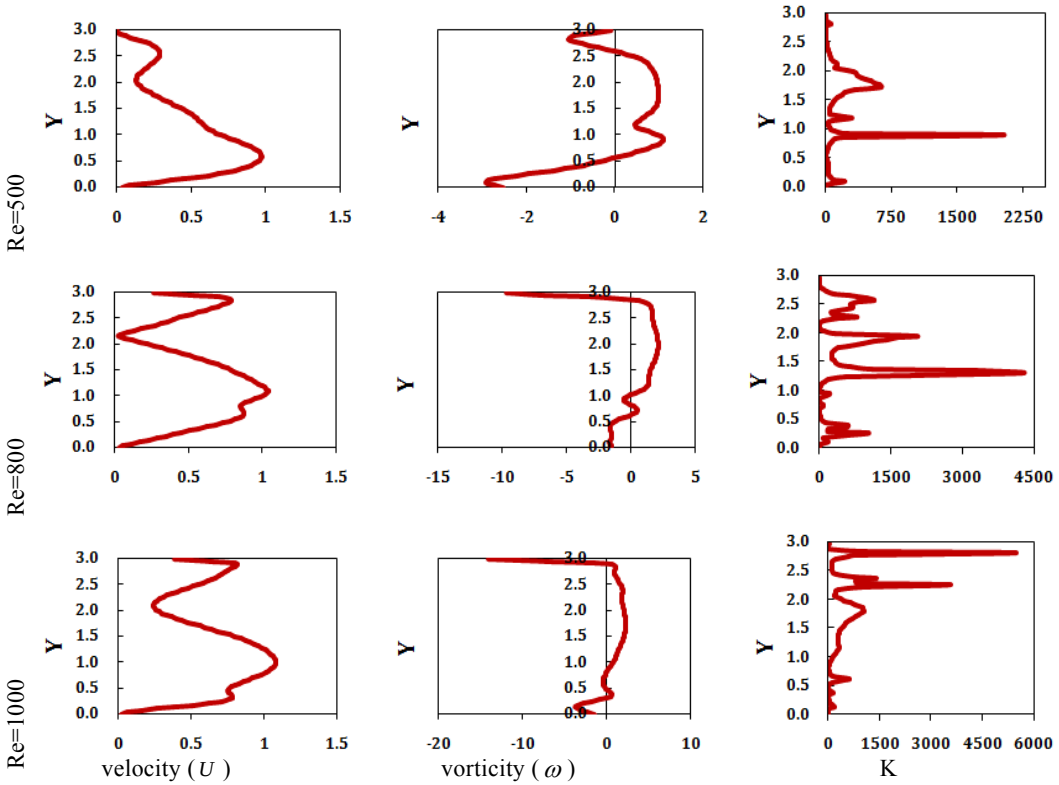


**Fig. 11. Distribution of velocity, vorticity and $K$ at section 3 at different Reynolds numbers of ranging from 500 to 1000 and expansion ratio of $H / h_i = 3$ .**

**Table 4 Position and value of $K_{max}$ under different Reynolds numbers ranging from 50 to 1000 and expansion ratios of $H / h_i = 1.9423$ and $H / h_i = 3$**

| case | | Reynolds number | | | | | |
|---|---|---|---|---|---|---|---|
| | | 50 | 100 | 300 | 500 | 800 | 1000 |
| $H / h_i = 1.9423$ | $K_{max}$ | 679.736 | 1153.490 | 3599.850 | 5995.670 | 9930.330 | 12551.800 |
| | X | 5.279 | 5.599 | 5.133 | 6.883 | 5.425 | 7.612 |
| | Y | 1.00 | 1.00 | 1.00 | 1.029 | 1.029 | 1.029 |
| $H / h_i = 3$ | $K_{max}$ | 596.478 | 1327.880 | 3976.010 | 6021.440 | 11421.800 | 15119.500 |
| | X | 5.395 | 5.337 | 5.308 | 7.00 | 5.716 | 9.362 |
| | Y | 2.069 | 2.099 | 2.099 | 2.099 | 2.130 | 2.220 |

expansion ratio (Biswas *et al.* 2004). As a results, according to Eqs.(7) and (8), by increase of pressure drop, we have larger energy gradient in transverse (or cross-stream) which leads to increase of K value.

## 4. CONCLUSION

We investigated the hydrodynamic instability of 2D BFS flow at six different Reynolds numbers ranging from 50 to1000 and two expansion ratios of 1.9423 and 3 by using energy gradient method. We compared our results with existing experimental and numerical data and good agreement is obtained. Three main conclusions of the present study are deduced as follows:

(1) As the expansion ratio decreases, the value of $K_{max}$ decreases, therefore, we expect that by reducing the expansion ratio, flow become more stable.

(2) Value of energy gradient function K at the corner eddy and recirculation zones is significantly low and therefore, these regions aren't the candidate of the onset instability in a BFS flows.

(3) We found that the values of $K_{max}$ occur on the separated shear layer nearby the step edge and

therefore, the origin of instability in the entire flow field of a two-dimensional backward facing step is located on the separated shear layer nearby the step edge.

One can be concluded that, energy gradient method has remarkable capability to study of flow filed stability. In addition, the current research merits further study in future. Investigation of the hydrodynamic instability of 3D BFS flow by using energy gradient method can be considered in future works.

## REFERENCES


Armaly, B. F., F. Durst, J. C. F. Peireira and B. Schönung (1983). Experimental and theoretical investigation of backward-facing step flow. *Journal of Fluid Mechanics* 127, 473–496.

Asgari, E. and M. Tadjfar (2017). Assessment of four inflow conditions on large-eddy simulation of a gently curved backward-facing step. *Journal of Turbulence* 18, 61–86.

Barkley, D., M. G. M. Gomes and R. D. Henderson (2002). Three-dimensional instability in flow over a backward-facing step. *Journal of Fluid Mechanics* 473, 167–190.

Bayraktar, S. (2014). Numerical solution of three-dimensional flow over angled backward-facing step with raised upper wall. *Journal of Applied Fluid Mechanics* 7(1), 155–1677.

Beaudoin, J. F., O. Cadot, J. L. Aider and J. E. Wesfreid (2004). Three-dimensional stationary flow over a backward-facing step. *European Journal of Mechanics-B/Fluids* 23(1), 147–155.

Biswas, G., M. Breuer and F. Durst (2004). Backward-facing step flows for various expansion ratios at low and moderate Reynolds numbers. *Journal of Fluids Engineering* 126, 362–374.

Blackburn, H. M., D. Barkley and S. J. Sherwin (2008). Convective instability and transient growth in flow over a backward-facing step. *Journal of Fluid Mechanics* 603, 271–304.

Bolgar, I., S. Scharnowski and C. J. Kähler (2015). Control of the reattachment length of a transonic 2D backward-facing step flow. *In Proceedings of the 5th International Conference on Jets, Wakes and Separated Flows*, Stockholm, Sweden.

Chiang, T. P. and T. W. H. Sheu (1999). A numerical revisit of backward facing step flow problem. *Physics of Fluids* 11(4), 862–874.

de la Torre, M., A. Acosta-Zamora, N. D. Love and A.R. Choudhuri (2017). Study of high intensity turbulent flow over a backward facing step using 10kHz particle image velocimetry. *In Proceedings of the 55th AIAA Aerospace Sciences Meeting*, Texas, USA.

Dou, H. S. (2004). Energy gradient theory of hydrodynamic instability. *The Third International Conference on Nonlinear Science*, Singapore.

Dou, H. S. (2006). Mechanism of flow instability and transition to turbulence. *International Journal of Non-Linear Mechanics* 41(4), 512–517.

Dou, H. S. and A. Q. Ben (2015). Simulation and instability investigation of the flow around a cylinder between two parallel walls. *Journal of Thermal Science* 24(2), 140–148.

Dou, H. S., B. C. Khoo and K. S. Yeo (2008). Instability of Taylor-Couette flow between concentric rotating cylinders. *International Journal of Thermal Science* 47(11), 1422–1435.

Erturk, E. (2008). Numerical solutions of 2-D steady incompressible flow over a backward-facing step, part I: high Reynolds number solutions. *Computers & Fluids* 37(6), 633–655.

Farahbakhsh, I., S. S. Nourazar, H. Ghassemi, H. S. Dou and A. Nazari Golshan (2014). On the instability of plane Poiseuille flow of two immiscible fluids using the energy gradient theory. *Journal of Mechanics* 30(3), 299–305.

Fortin, A., M. Jardak, J. J. Gervais and R. Pierre (1997). Localization of Hopf bifurcations in fluid flow problems. *International Journal for Numerical Methods in Fluids* 24(11), 1185–210.

Gartling, D. K. (1990). A test problem for outflow boundary conditions-flow over a backward-facing step. *International Journal for Numerical Methods in Fluids* 11(7), 953–967.

Huang, R., X. Luo, B. Ji and Q. Ji (2017). Turbulent flows over a backward facing step simulated using a modified partially averaged Navier–stokes model. *Journal of Fluids Engineering* 139(4), 1–7.

Kaiktsis, L., G. E. Karniadakis and S. A. Orszag (1991). Onset of the three-dimensionality, equilibria, and early transition in flow over a backward facing step. *Journal of Fluid Mechanics* 231, 501–528.

Kaiktsis, L., G. E. Karniadakis and S. A. Orszag (1996). Unsteadiness and convective instabilities in two-dimensional flow over a backward-facing step. *Journal of Fluid Mechanics* 321, 157–187.

Kim, J. and P. Moin (1985). Application of a fractional-step method to incompressible Navier–stokes equations. *Journal of computational physics* 59(2), 308–323.

Kosma, Z. (2005). Method of lines for the incompressible Navier-stokes equations in the stream-function formulation. *TASK Quarterly* 9(1), 17–35.

Li, Y., J. I. Choi, Y. Choic and J. Kim (2017). A simple and efficient outflow boundary condition for the incompressible Navier–stokes equations. *Engineering Applications of Computational Fluid Mechanics* 11(1), 69–85.

Nishioka, M. and Y. Ichikawa (1975). An experimental investigation of the stability of plane Poiseuille flow. *Journal of Fluid Mechanics* 72(4), 731–751.

Rajasekaran, J. (2011). *On the flow characteristics behind a backward-facing step and the design of a new axisymmetry model for their study*. Ph. D. thesis, the University of Toronto, Ontario, Canada.

Troutt, T. R., B. Scheelke and T. R. Norman (1984). Organized structures in a reattaching separated flow field. *Journal of Fluid Mechanics* 143, 413–427.

Xie, W. A. and G. N. Xi, (2017). Fluid flow and heat transfer characteristics of separation and reattachment flow over a backward-facing step. *International Journal of Refrigeration* 74, 175–187.